Available online at www.sciencedirect.com
ScienceDirect
Dyes and Pigments 76 (2008) 406–416
DYES and PIGMENTS
www.elsevier.com/locate/dyepig

An insight into the mechanism of the cellulose dyeing process: Molecular modelling and simulations of cellulose and its interactions with water, urea, aromatic azo-dyes and aryl ammonium compounds

Mark S. Baird [a], John D. Hamlin [b], Antoinette O'Sullivan [a], Andrew Whiting [b,*]

[a] *Department of Chemistry, University of North Wales at Bangor, Wales, UK*
[b] *Department of Chemistry, University of Durham, Science Laboratories, South Road, Durham DH1 3LE, UK*

Received 7 July 2006; accepted 25 September 2006
Available online 5 December 2006

Abstract

Potential cellulose-surface active aryl ammonium compounds that may also de-aggregate dye molecules in aqueous solution have been modelled using molecular mechanics methods and simulation methods, and compared with known additives such as amines and urea, as an extrapolation of modelling the interaction of water and urea molecules with cellulose microfibril surfaces. The results from these modelling studies have clearly elucidated the way in which polar molecules interact with cellulose surfaces, and have been used to provide insight into the dyeing process and to identify which new molecular systems might be predicted to act as molecular delivery agents for assisting dye processes.

Keywords: Cellulose; Dying; Mechanism; Additives; Molecular simulation

1. Introduction

The molecular structure of cellulose has been studied over the years by a number of techniques such including molecular modelling [1], FT-IR [2], solid state Cross Polarisation/Magic Angle Spinning (CP/MAS) NMR [3], solid state ^{13}C NMR [4], neutron [5] and electron [6] diffraction, Raman spectroscopy [4], scanning [7] and transmission electron microscopies and atomic force microscopy (AFM) [8]. These techniques have aided in the elucidation of the structure of cellulose. However, the structure is complex because the crystalline properties of cellulose vary with the source, the amorphous nature of the source and the number of polymorphs present in the source. It is not the intention to review the cellulose structure because recent reviews are available in the literature [9].

Cotton is the purest natural form of native cellulose with a cellulose I polymorphic structure. This cellulose I polymorph can readily undergo interconversion to other polymorphs. The cellulose II polymorph interconversion being initiated by mercerisation; a technique common in the textile industry whereby cellulose is exposed to concentrated sodium hydroxide solution. Computational analysis of cellulose over the decades has had varying degrees of constraint applied to reduce the computational power and time required [10]. As molecular mechanics force fields have evolved, the constraints applied to the original models have been largely removed.

Computational analysis of cellulose has been undertaken by many groups [11–13], with varying degrees of success. With this in mind, we did not want to repeat the work of other groups by modelling cellulose, but to use the models already available for studying the interactions of the cellulose matrix with dyes and solvent molecules at the molecular level. The initial model that we intended to use in our studies was that of Hardy [11] (Fig. 1). This structure consists of a planar

* Corresponding author. Tel.: +44 191 334 2081; fax: +44 191 384 4737.
E-mail address: andy.whiting@durham.ac.uk (A. Whiting).

0143-7208/$ - see front matter © 2006 Elsevier Ltd. All rights reserved.
doi:10.1016/j.dyepig.2006.09.011

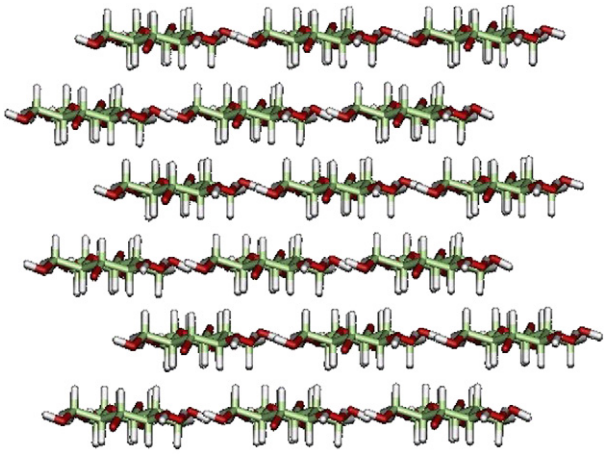

Fig. 1. End view of the Hardy planar array.

3 × 6 array of strands, each strand being eight glucose residues in length (Fig. 2).

However, this proved to be impractical since these cellulose block models did not appear to have the characteristics of a cellulose microfibril, which has been described as being nearly square with lateral dimensions of 3–4 nm [12] and would contain 36 chains. Hence, we have adopted [1] models produced by Baird et al. [14]. These models were all based on cellulose I literature dimensions [12] and was sufficiently large to mimic a cellulose microfibril, with the desired characteristics outlined above. It was therefore our intention to use this structure, along with other molecular modelling tools, such that additives could be designed and tested in a conceptual manner before any synthetic work was undertaken. The main tool of choice for this study was interaction mapping tool within Quanta 97®. One of the options of the interaction mapping is the facility to probe a structure with a second structure. In this paper on the modelling of cellulose in water and on the mechanism of the cellulose dyeing process, we provide an insight into cellulose–water interactions which is of utmost importance with respect to the processing of cellulose for dyeing applications. It is shown that cellulose does not wet in an even fashion but with clustering of water in certain regions. We also study the behaviour of potential dye-bath additives and dye molecules in the vicinity of cellulose and their interactions using the probe map tools within Quanta 97®.

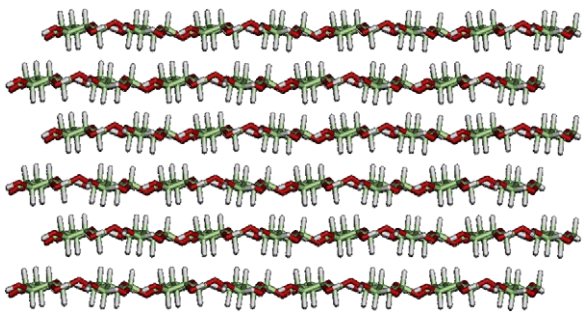

Fig. 2. Side view of the Hardy planar array.

2. Methods

Dyes and all potential additives, with the exception of water and cellulose molecules, were initially drawn within the 2D molecular builder available within Quanta 97®, using the Baird et al.'s approach [14]. These structures were then minimised (gas phase) such that each component in the more complex models was at its own gas phase local minimum. The potential additives were initially constructed and minimised using molecular mechanics (see Section 5), before being subjected to gas phase molecular dynamics simulations and simulated annealing *via* re-minimisation. The minimised structures obtained were then used for probe mapping studies.

Solvated models were constructed by combining the desired structures before solvation using the solvation tools available within Quanta 97®. These tools involve the incorporation of each water molecule, as opposed to there being simulated solvation using a dielectric constant.

The cellulose models of Baird and O'Sullivan [14] were initially minimised using molecular mechanics (see Section 5), before use with Quanta 97®. All structures were subjected to minimisations using the SD method to remove bad contacts, then CG minimisations over 4000 iterations. This conjugate gradient minimisation regime was repeated where necessary until convergence had occurred, with a convergence limit set at the default value of 0.01 kcal mol^{-1}. The minimised structures were then subjected to molecular dynamics simulations, followed by simulated annealing *via* re-minimisation.

Probe maps were performed as outlined (see Section 5), using the interaction mapping menu within Quanta 97®. The cellulose matrix [15] and the chosen additive were then placed apart in space, with the additive selected as the probe, and the cellulose matrix selected as the structure to be probed. The probe mapping was performed within the confines of a 10 Å box, between the energy limits of +100 kcal mol^{-1} and −200 kcal mol^{-1} and the resulting probe maps were displayed as a grid around the cellulose matrix.

3. Results and discussions

To comply with the specifications for a celluose microfibril, *i.e.* nearly square with lateral dimensions of 3–4 nm and containing approximately 36 chains, Baird and O'Sullivan [14] constructed a model of a cellulose microfibril from a monoclinic unit cell of cellulose I, which consisted of two chains, each eight glucopyranose units in length. To remain within the constraints of the modelling package and computational power used, a 16 chain model of a microfibril was constructed as shown in Figs. 3 and 4 and not the desired 36 chain. In Fig. 3 the non-reducing chain ends of the microfibril can be seen, whilst Fig. 4 displays the length of the chains with the non-reducing ends orientated to the right of the model.

This model, although somewhat smaller than a cellulose microfibril, was suitable for our needs since it contains surface and non-surface chains, *i.e.* it has a central core not exposed to the outside environment and also has a reducing end and non-reducing end, allowing full exploration of the microfibril. This

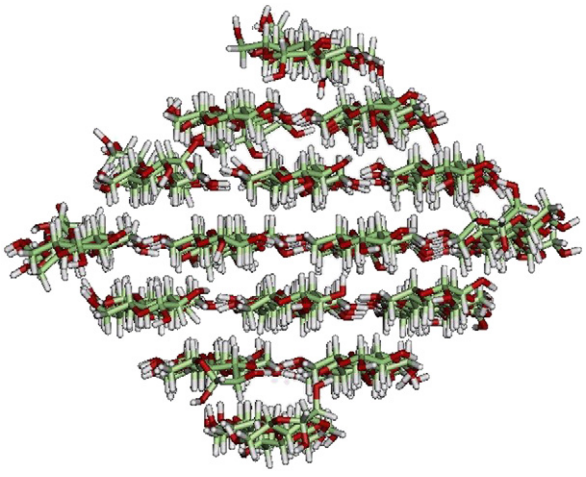

Fig. 3. End view of the non-reducing end of 16 × 8 array of cellulose.

reduction in size allowed computational calculations to be performed at reasonable speed. The microfibril has dimensions of 21 × 21 × 45 Å, and a total energy of −2039.74 kcal mol^{-1} after minimisation and a final energy of −2532.1 kcal mol^{-1} following 5 ps of dynamics simulation and simulated annealing. After re-minimisation within Quanta 97® this annealed structure had an energy of 1344.04 kcal mol^{-1}, which although somewhat different from that reported by Baird et al. [14], is accounted for in that the energy observed is specific to the modelling package and the force field used.

Cellulose–water interactions have been extensively studied by various techniques, including IR-spectroscopy [13], NMR [15], and sorbtion isotherms [16]. In crystalline cellulose I, there are many sites at which water sorbtion can occur due to the large number of hydroxyls on the surface. The energy minima of the sorbtion sites vary due to the relative balance of attractive and repulsive forces, localised steric hindrance, position of interfering atom groups, possibility of water bound to more than one substrate group, and interference from other water molecules [17]. It is also known that water in contact with macromolecules behaves differently to water in the bulk of a solution. This difference can be attributed to sorbtion and disruption of the hydrogen-bond network in the water, in that water molecules are hydrogen bonding to the carbohydrate hydroxyls as opposed to other water molecules [18].

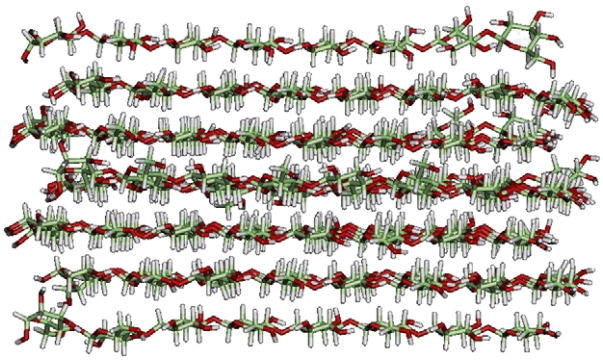

Fig. 4. Side view of 16 × 8 array non-reducing end of cellulose, orientated to the right.

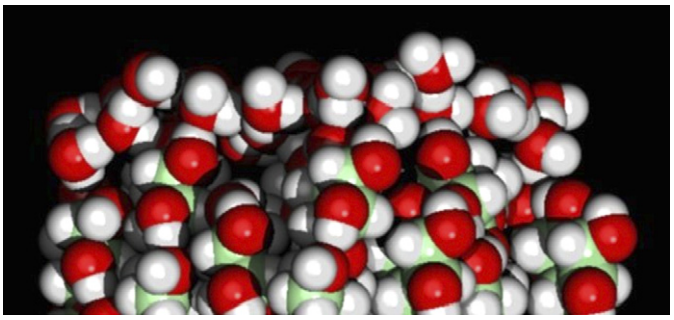

Fig. 5. Side view of the solvated, non-reducing end of a 16 × 8 cellulose matrix.

Baird and O'Sullivan [19] performed complex modelling studies involving end solvation (Fig. 5) and side solvation (Fig. 6). They found that cellulose does not wet evenly over the whole structure, but has regions with a high solvation affinity and areas with a low solvation affinity, as proposed by Pizzi and Eaton [17]. These higher affinity sorbtion sites lead to a clustering of water molecules, since it appears that it is more favourable for water molecules to bond to water molecules at a high affinity site than to bond to cellulose at a lower affinity site. This leads to an interesting discussion on the nature of water layers forming on cellulose. Hartley et al. [20] stated that water molecules at a hydration site may interact with each other to form clusters, as it is the natural tendency of water [21].

Modelling work performed during this study by Baird et al. and O'Sullivan [14,19] with 55 water molecules placed over the non-reducing end of the 16 × 8 matrix (Fig. 5) found that 38% of the water molecules get 'sucked in' towards the end of the matrix. Three 'kinds' of water were observed in this study; *i.e.* (1) water bound to cellulose; (2) water clustering to bound water; and (3) free water molecules. These observations support the selective wetting discussed above.

Solvation of the side of the matrix affords water molecules the chance to move along the side of the matrix, to find a higher affinity sorbtion site resulting in clustering of the water molecules at the end of the cellulose microfibril model, and thus minimising the degree along the microfibril, in

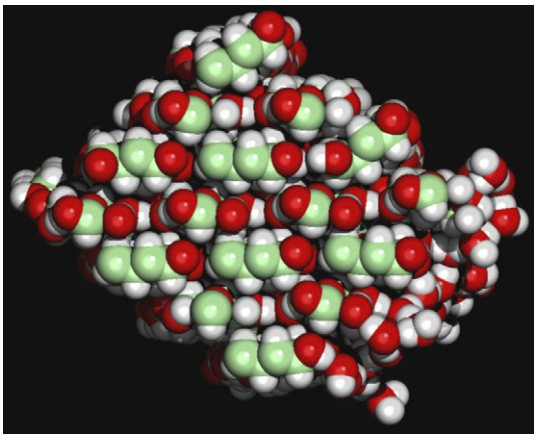

Fig. 6. Non-reducing end view of the side of cellulose solvated (16 × 8 cellulose matrix).

accordance with the proposals of Pizzi and Eaton [17], and Hartley et al. [20]. This was also observed by Baird and O'Sullivan [19], as depicted in Fig. 6.

It can be seen from the above modelling studies that cellulose–water interactions are reasonably well understood if not completely documented, and that there was little need to reproduce these results within Quanta 97®. We did, however, check that provided similar results for the minimisations and dynamics simulations of the 16 × 8 cellulose matrix and that water on the side face behaved as predicted by our co-workers. This work was carried out as outlined in Section 5 to produce the results predicted in Fig. 7. In this paper, we extend these studies to provide an insight into what happens in the presence of urea within the textile processing industry.

3.1. Computational analysis of cellulose with amines and urea

Ammonia has been investigated in relation to colour changing properties [22] and swelling of wood [23]. This application of anhydrous liquid ammonia in conjunction with sodium hydroxide in an attempt to overcome the difficulty of mercerising natural fibres, such as jute [24], interested us. Molecular dynamics studies by our co-workers showed that a pressure of 500 atm was required before ammonia molecules entered the cellulose matrix. The familiar hydrogen bonding and clustering interactions of ammonia molecules were being prevalent below the extreme pressure indicated (Fig. 8).

Our molecular dynamics studies were concerned with cellulose–urea interactions and especially, those interactions on the side face of the matrix, since these make up more of the active surface area within a cellulose microfibril. These studies were initially performed in the gas phase, with the urea molecules (18 of them) being randomly placed around the junction of two of the side faces. It was observed that the urea molecules hydrogen-bond both with themselves and with the cellulose matrix, leading to a distortion of the most exposed strand (shown on the left hand side of Fig. 9).

The hydrogen bonding of urea to the cellulose matrix takes place through the available C(2)-, C(3)-, and C(6)-position hydroxyl groups, with urea–urea interactions acting through the carbonyl of one urea and amide hydrogens of an adjacent urea molecule. These hydrogen-bonding interactions can be seen from the close up of Fig. 9, as shown in Fig. 10, and from above Fig. 9, as depicted by Fig. 11.

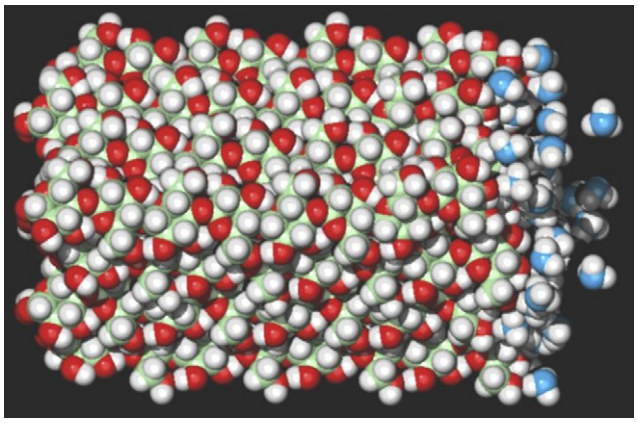

Fig. 8. Space fill view of the clustering of ammonia around the non-reducing end of 16 × 8 cellulose array [21].

It has been suggested that urea, amongst other effects, behaves as a swelling agent [25], causing the swelling of the cellulose matrix, thus facilitating the ingress of the dye. This may be the case with bulk cellulose, *i.e.* expansion of the inter-microfibrillar space would allow the ingress of dye into the deeper, more secluded fixation sites. However, this swelling does not appear to extend to the microfibrillar level, from the results obtained here, since we observe no ingress of the urea into the matrix and only minor deformation of the exposed edge of the cellulose matrix.

3.2. Computational analysis of C.I. Reactive Red 2 (Procion Red MX-5B) with cellulose

Dye–cellulose interactions have been studied by placing the dye molecules in question (two molecules of C.I. Reactive Red 2) in close proximity to the stripped down and

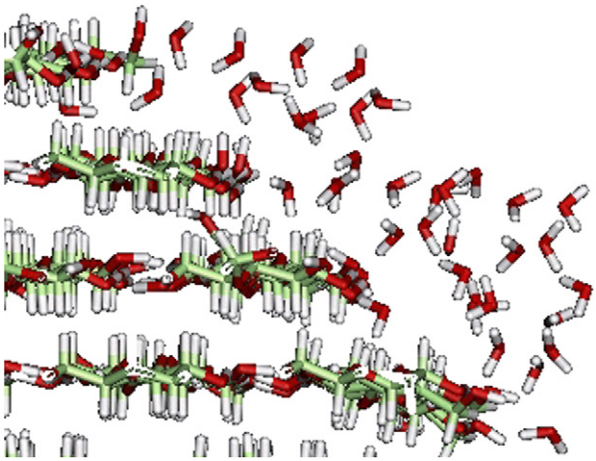

Fig. 7. Cellulose–water interactions.

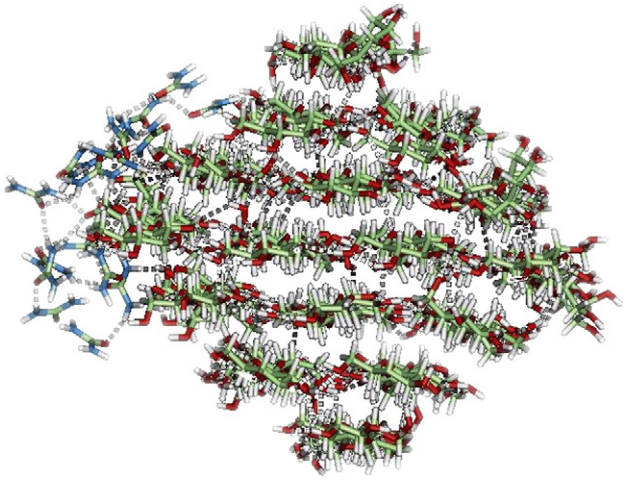

Fig. 9. Gas phase dynamics simulation of 16 × 8 cellulose matrix with urea.

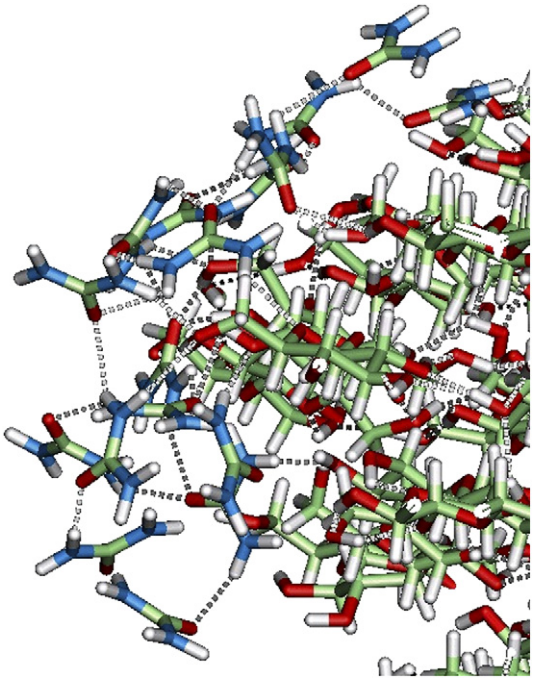

Fig. 10. Close up view of the hydrogen-bonding network in from Fig. 9.

re-minimised 16 × 8 cellulose matrix, and performing aqueous phase molecular dynamics simulations as shown in Fig. 12. Molecular dynamics simulations were performed after the addition of a 10 Å solvation sphere to all residues. This was performed as outlined in Section 5. Minimisation studies were also performed, along with the molecular dynamics simulations; however, no firm patterns have emerged as to where the C.I. Reactive Red 2 dye molecules prefer to be orientated in relation to the cellulose matrix (Figs. 13 and 14). This may suggest that there is no apparent specificity in the initial dye–cellulose binding process. In fact there appears to be minimal interaction of any kind between dye and cellulose surface, however, given the fact that water molecules tend to cluster in specific regions around the cellulose matrix and that the

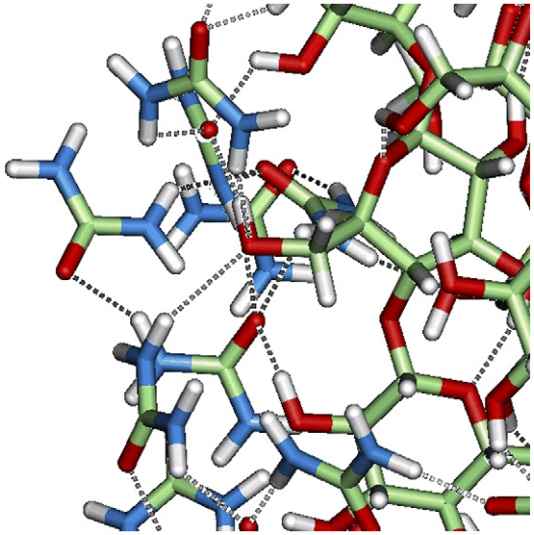

Fig. 11. A further close up view of Fig. 10.

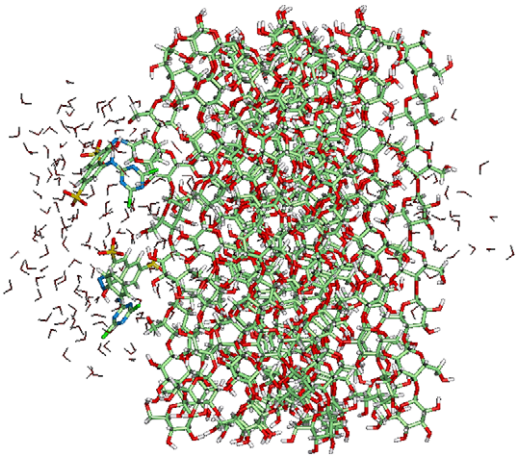

Fig. 12. Dye–cellulose orientation shown from above the matrix.

dye is 'dissolved' in water, it could be envisaged that there is likely to be an effective and selective delivery process operating, based entirely upon greatest cellulose–water interactions. If this is the case, one would expect dye–cellulose interactions to be maximal where the cellulose–water interactions are maximal, *i.e.* at amorphous regions, at dislocations of the crystalline structure, *i.e.* at the strand ends and microfibril edges, and around the more available 6-position hydroxyl groups in those areas.

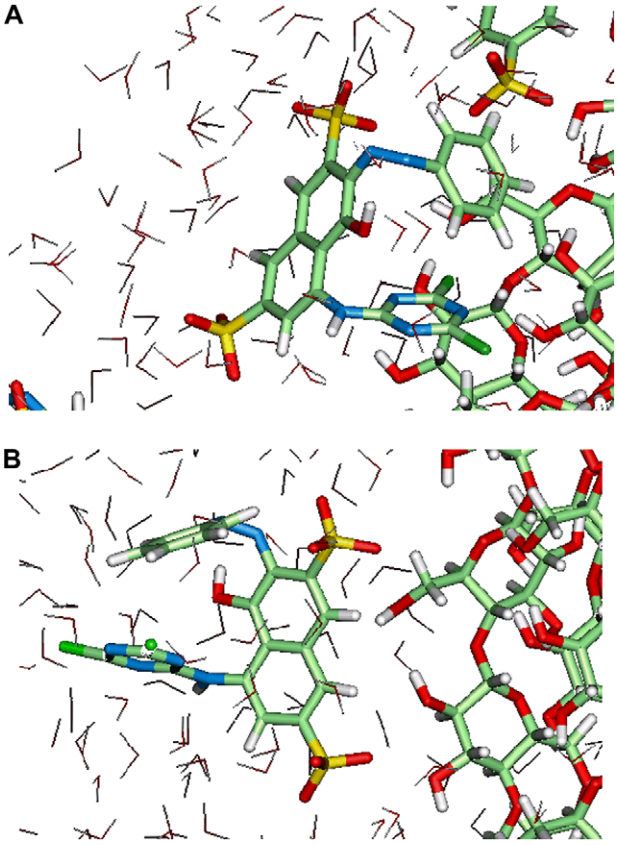

Fig. 13. (A) Dye–cellulose orientation about the reactive function and the C(6) hydroxyl. (B) Showing the lack of specificity in the orientation of the C.I. Reactive Red 2 with the cellulose matrix.

3.3. Computational analysis of cellulose with potential additives

The interactions between the cellulose and potential additives were observed and modelled by use of probe interaction techniques. This was done since the demand placed on computational time by these systems was large if meaningful results were to be generated by molecular dynamics simulations. Probe interaction calculates empirical energy field maps. A probe molecule or atom (in our case the additive in question) is used to sample the chosen environment. As the structure is probed, the energy is calculated between the probe and target at all points within the pre-defined sampling box. The energy calculated is the Lennard–Jones van der Waals energy, the electrostatic energy, or the sum of both the energies.

For molecular interaction studies, the probe is tumbled about the target at specified angles and increments and an energy calculation performed at each point of a grid superimposed on the target, using all possible combinations of probe rotation angles. A contour map is calculated by taking the maximum and minimum energy values for each grid point (Fig. 15).

The probe map studies of the mono-ammonium species *i.e.* aniline hydrochloride **1**, benzylamine hydrochloride **2**, 4-methoxybenzylamine hydrochloride **3** and 2-(3,4-dimethoxyphenyl)ethylamine hydrochloride **4** seem to infer that the introduction of the extra carbons and the methoxy moieties to the initial phenyl core lead to more favourable interactions between the additive species and the cellulose matrix. The probe map displayed in Fig. 16 for aniline **1** and cellulose was probed within the confines of a 15 Å box. It can be

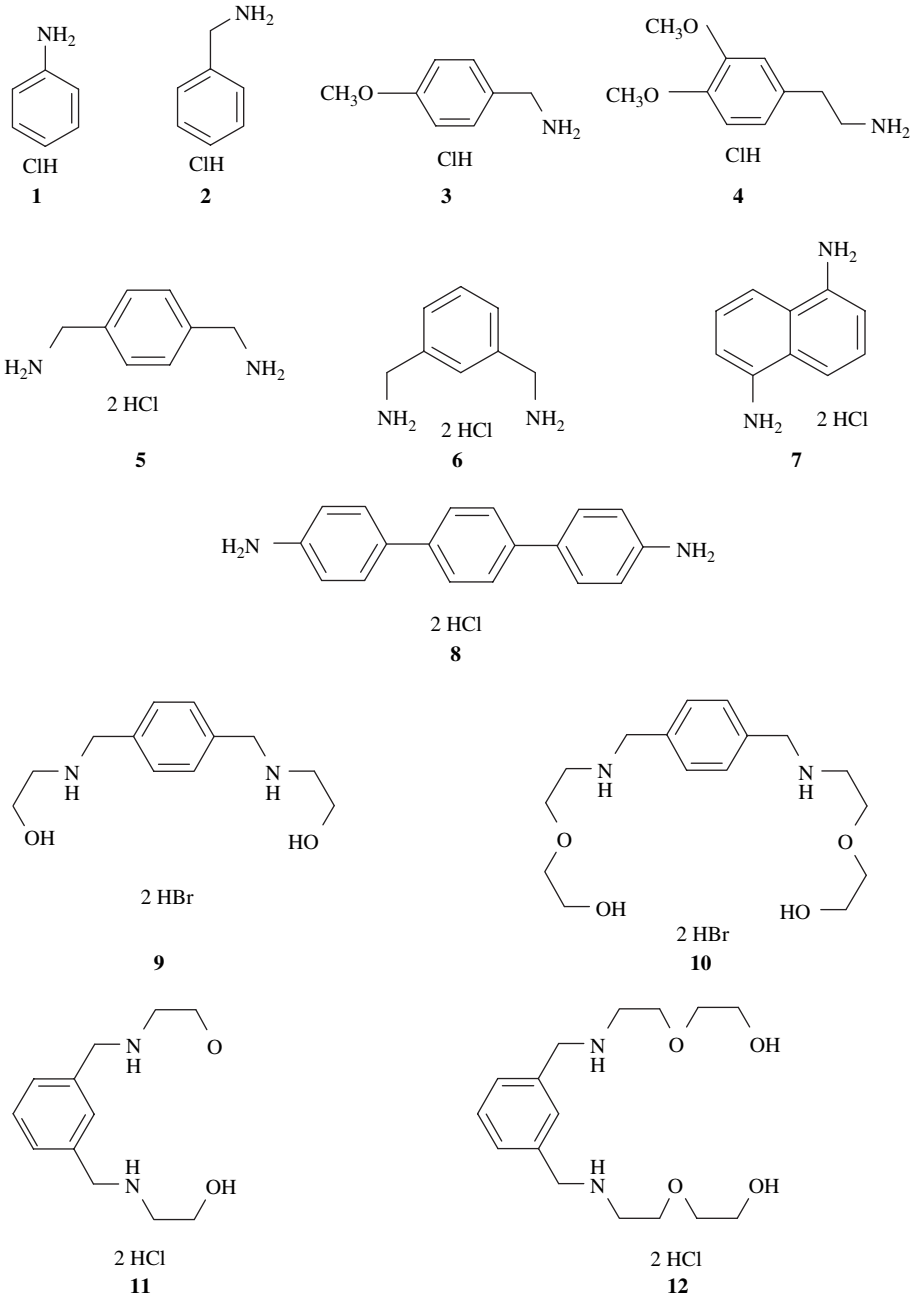

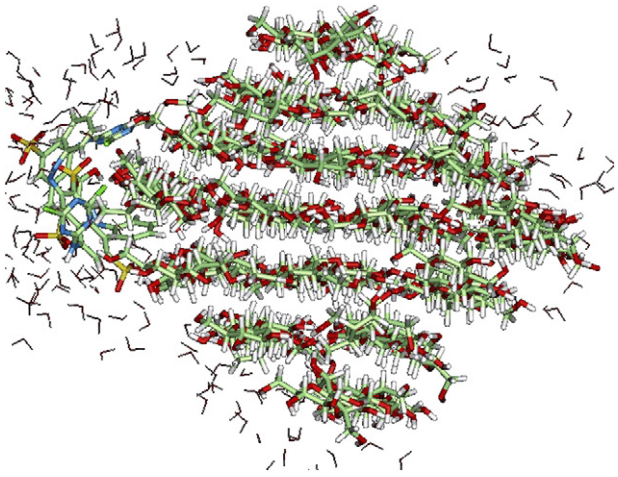

Fig. 14. End view showing orientation of dye with cellulose.

seen from the red matrix that close interaction over most of the cellulose matrix is energetically unfavourable, whilst the blue matrix, which indicates favourable interactions, has an energy of $-115.78\ \mathrm{kJ\ mol^{-1}}$ and covers much less of the cellulose surface.

If we look at the probe map of benzylamine hydrochloride **2** (Fig. 17) with the cellulose, we see that the red (energetically unfavourable interaction) matrix once again envelopes the cellulose. However, the blue (energetically more favourable interaction) matrix can be seen to be permeating the probe map with particularly favourable interactions occurring above and below the cellulose hydroxyls. This is even more pronounced with 4-methoxybenzylamine hydrochloride **3** (Fig. 18) and 2-(3,4-dimethoxyphenyl)ethylamine hydrochloride **4** (Fig. 19) probe maps, thus indicating that the addition of the methoxy groups, which were incorporated to increase solubility, has a favourable effect upon the cellulose–additive recognition and binding processes according to the modelling studies.

The probe map studies for the initial di-ammonium series of additives included *p*-xylenediamine dihydrochloride **5**, *m*-xylenediamine dihydrochloride **6**, 1,5-diaminonaphthalene dihydrochloride **7** and diaminoterphenyl dihydrochloride **8**.

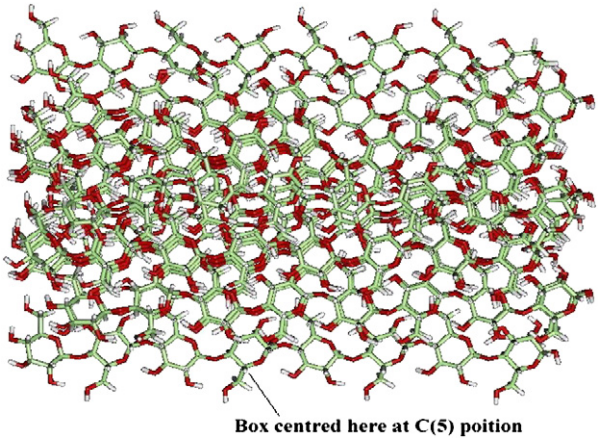

Fig. 15. Figure showing the position of the probe map box centred on the C(5) carbon indicated.

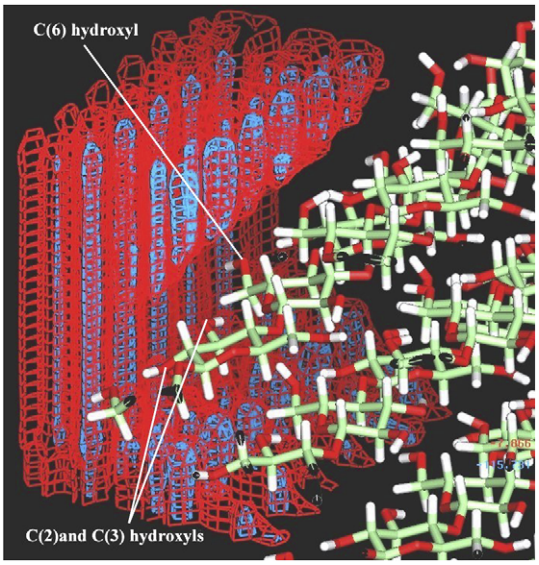

Fig. 16. Probe map of aniline hydrochloride **1** on cellulose.

If we look at the probe map for *p*-xylenediamine dihydrochloride **5** on cellulose (Fig. 20) we can see that the red matrix, *i.e.* unfavourable interaction matrix, has diminished and there appears to be much more evidence of favourable interaction (blue matrix) between the additive and the cellulose matrix. It is also apparent that the distance between the red and blue matrices has decreased significantly, indicating that the additive is now able to get within close proximity to the cellulose before repulsions begin to take effect thus facilitating the hydrogen-bonding interactions between the additive and the cellulose. We are now beginning to see a continuation of the blue matrix around most of the cellulose as opposed to the channels seen previously with the mono-ammonium species congregating around the cellulose hydroxyls. All these indicate that the approach to additive design appears to be generating better target structures with each cycle.

If we compare the probe map of *p*-xylenediamine dihydrochloride **5** (Fig. 20) with that of benzylamine hydrochloride **2** (Fig. 16), we can see that both the plots envelop the cellulose in a similar manner. Although, the extra interaction obtained from the addition of the second alkyl ammonium in the

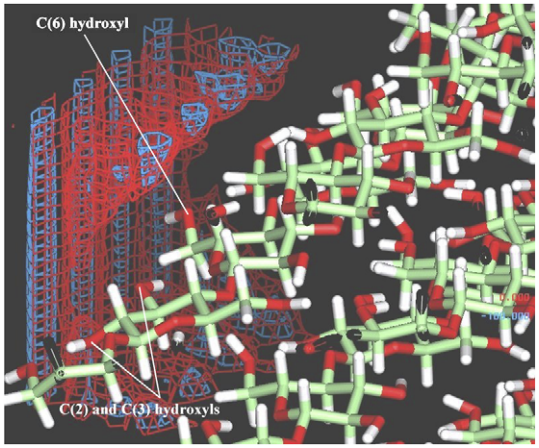

Fig. 17. Probe map of benzylamine hydrochloride **2** on cellulose.

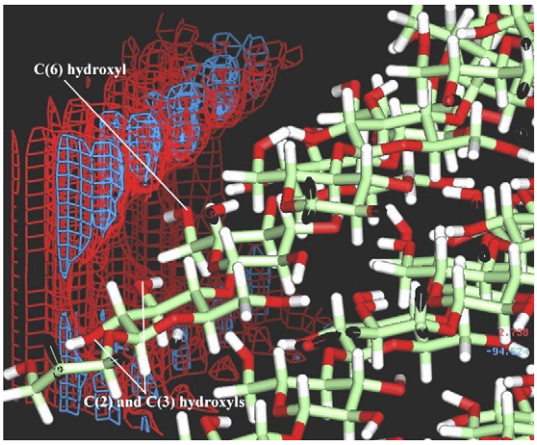

Fig. 18. Probe map of 4-methoxybenzylamine hydrochloride **3** on cellulose.

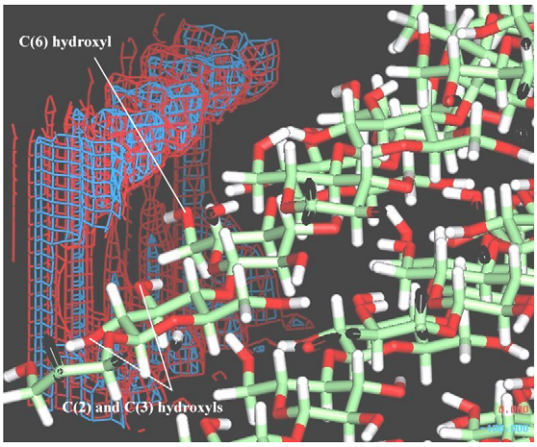

Fig. 20. Probe map of *p*-xylenediamine dihydrochloride **5**.

para-position has an effect that is much greater than one would have anticipated from the previous results.

The relocation of the second alkyl ammonium moiety to the *meta*-position (Fig. 21) leads to a probe interaction map that is somewhat more complicated than was the case for the *p*-xylenediamine dihydrochloride. This is manifested by the fact that we now have an abundance of blue (favourable) channels and what appears to be a compromise between Figs. 17 and 20. As a result we would expect that this additive would perform in some intermediate capacity between that of the benzylamine hydrochloride **2** and the *p*-xylenediamine dihydrochloride **5**.

The probe maps for the 1,5-diaminonaphthalene dihydrochloride **7** (Fig. 22) and diaminoterphenyl dihydrochloride **8** (Fig. 23) seem to indicate that these two di-ammonium species would perform to a lesser degree than the *m*- and *p*-xylenediamine dihydrochloride species, **6** and **5**, respectively. This may be due to the increased hydrophobicity imparted upon these additives by the larger organic core; however, there still appears to be definite interactions between the additives and the cellulose hydroxyl sites.

If we return to the *m*- and *p*-xylenediamine dihydrochloride species that appear from the preceding modelling exercises to be two potential candidates for salt replacement, we can look at the effect of these adding polyethyleneglycol (PEG) units to each of the terminal amines. The addition of these groups was carried out to increase the solubility of the additives such that they can be used at high concentrations if desired whilst simultaneously providing further sites for dye–cellulose binding interactions.

If we now compare the results obtained for *p*-monol **9** and *p*-digol **10**, Figs. 24 and 25, respectively, we can see that on going from one ethyleneglycol unit to two that the probe interaction maps with the cellulose matrix show an increase in the inability of the additive to interact with the cellulose matrix. This could possibly be attributed to steric factors and a masking of the ammonium functionality.

If we now compare these results with those of the initial *p*-xylenediamine dihydrochloride additive **5** we can see that there is an increasing lack of interaction on going from the *p*-xylenediamine dihydrochloride **5** to the *p*-monol **9** and again on going from the *p*-monol **9** to the *p*-digol **10**. This occurs to such an extent that the blue (favourable interaction) matrix in Fig. 24 for *p*-monol **9** has been displaced away from the cellulose array. Also, in the *p*-digol **10** case (Fig. 25) the blue

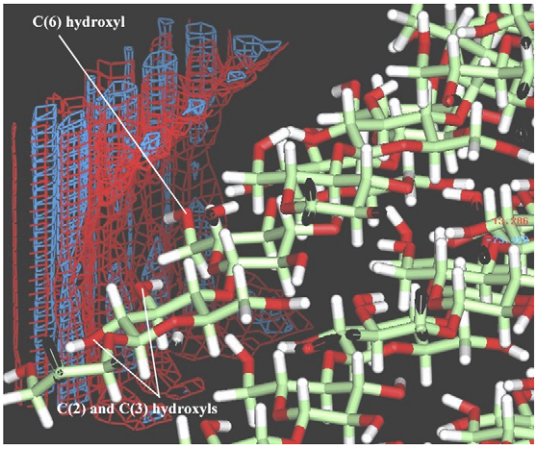

Fig. 19. Probe map of 2-(3,4-dimethoxyphenyl)ethylamine hydrochloride **4** on cellulose.

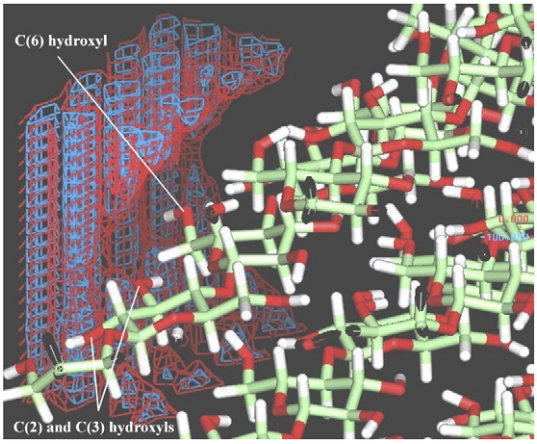

Fig. 21. Probe map of *m*-xylenediamine dihydrochloride **6**.

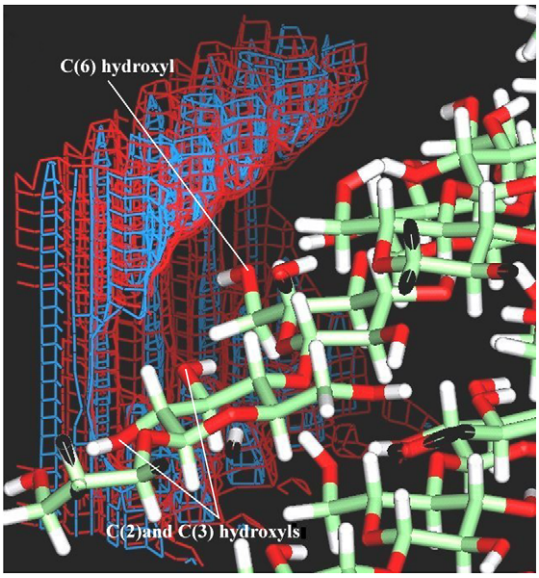

Fig. 22. Probe map of 1,5-diaminonaphthalene dihydrochloride **7** on cellulose.

and red matrices merely form a wall at the back of the probe sample box. Hence, it is envisaged that whilst these additive had already displayed strong interactions with the dyes, they would have little influence upon the binding to the cellulose.

Finally, if we look at the interactions between the cellulose and the *m*-xylenediamine dihydrochloride with the attached PEG moieties, *i.e.* *m*-monol **11** (Fig. 26) and *m*-digol **12** (Fig. 27), we see a similar trend to that observed for the *m*-xylenediamine dihydrochloride series. There is the same decrease in interaction between the additive and the cellulose array with the resultant probe mapping of only the back wall of the probe map box once again. This would therefore lead us to believe that these would be poor additives for the binding to cellulose, although once again they displayed excellent results

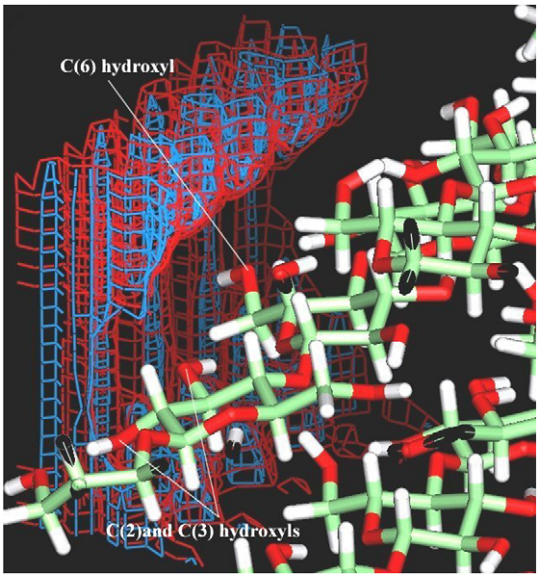

Fig. 23. Probe map of diaminoterphenyl dihydrochloride **8** on cellulose.

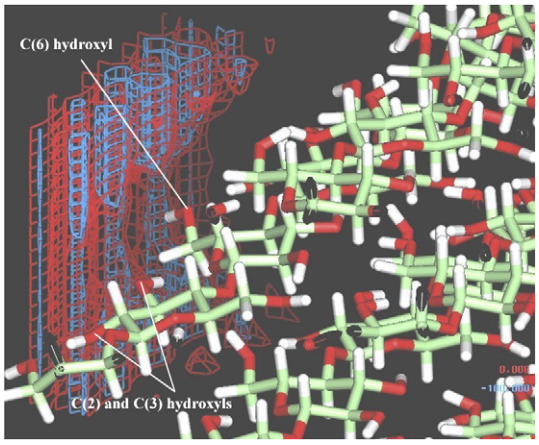

Fig. 24. Probe map of *p*-monol **9**.

with the binding of the dye, which is much enhanced by the PEG chains.

4. Conclusions

From the results presented above, it can be seen that the structure of cellulose is predictable using established models and that molecular modelling can be applied to generate representative 3D structures. In turn, these models can be used to examine certain molecular level phenomena, such as surface wetting and interactions with potential dye-bath additives. It is apparent from this work, and that of Pizzi et al. [17] and Baird and O'Sullivan [9,14,19], that cellulose does not wet evenly, in contrast, it has pockets of higher and lower affinities, and water forms hydrogen-bonded clusters around the higher affinity sites, whilst the lower affinity sites are devoid of major interactions.

We have shown that Quanta 97® can be used for these large structures with comparable results to larger software packages and have extended the molecular mechanics modelling of cellulose and water to include urea (as used in the textile industry) and have shown how urea facilitates the adsorption of water onto the cellulose microfibril surface. The modelling of dyes in the presence of cellulose has also been presented,

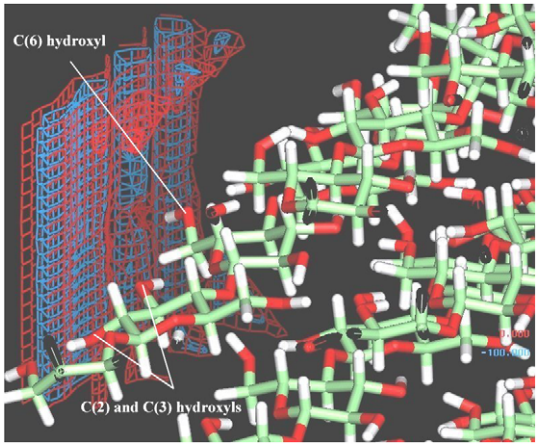

Fig. 25. Probe map of *p*-digol **10**.

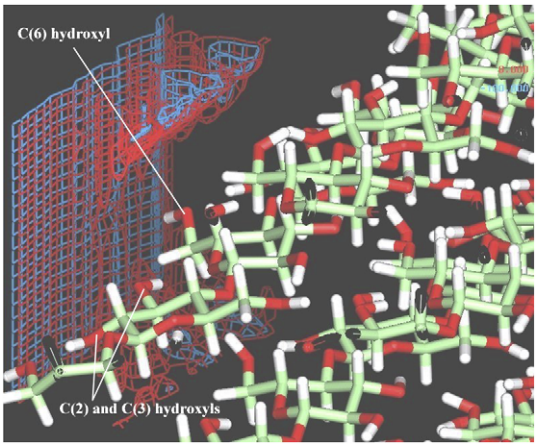

Fig. 26. Probe map of *m*-monol **11**.

and although no firm conclusions can be drawn as to the exact orientation of the dye in relation to the cellulose, we observe the approach of dye molecules to areas of cellulose where water molecules also cluster, *i.e.* around strand ends, and hence are in closest proximity to the free 6-position hydroxyl groups of glucosyl rings.

The probe mapping results infer that all of the above additives modelled herein show some level of interaction with the cellulose matrix, with the *m*- and *p*-xylenediamine dihydrochloride additives **6** and **5** in particular showing the strongest interactions and are therefore all viable targets for future synthesis and testing as potential dye-delivery agents. However, modelling of such additives and their interactions with cellulose also need to be balanced with their predicted (modelled) interactions with dyes. The combination of modelling both dye–additive and additive–cellulose interactions should allow one to predict which additives are truly suitable candidates for synthesis and application. In future work, we will report on these dye–additive interaction studies and experimental determination of the validity of this type of modelling approach to the rational design and application of dye-bath additives to improve dyeing efficiency.

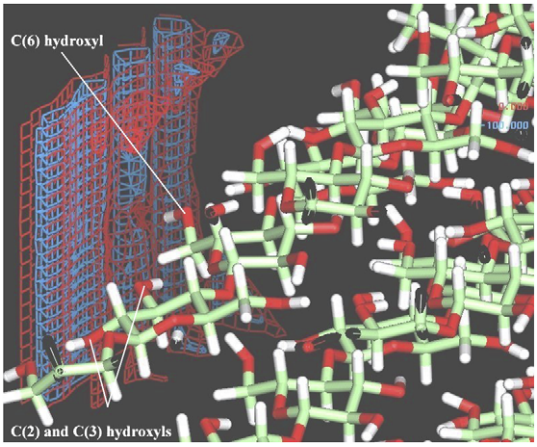

Fig. 27. Probe map of *m*-digol **12**.

5. Experimental procedures

5.1. General computational procedures

All molecular modelling work was undertaken on a Silicon Graphics O_2 workstation with a 180 MHz CPU, 64 MB of RAM running IRIX 6.2. Quanta® was used in the initial stages and was upgraded to Quanta 97®. Hardcopies of structures were prepared using Snapshot for screen capture and XV for RGB to JPEG conversion.

5.2. Gas phase minimisation studies of C.I. Reactive Red 2 (azo-phenol form)

A Procion Red MX-5B molecule was constructed using the 2D molecular editor interface within Quanta 97®. This was then subjected to gas phase minimisations over 4000 iterations using the steepest descent (SD) algorithm to remove high energy interactions, then the minimisation was repeated using the conjugate gradient (CG) algorithm again until the structure reached its minimum energy according to the CHARMm force field.

5.3. Gas phase molecular dynamics studies of C.I. Reactive Red 2 (azo-phenol form)

Using the CG minimisation output from procedure 1 molecular dynamics simulations were performed. The dynamics simulations were run over a 4 ps time scale, for each of the stages, heating to 300 K, equilibration and simulation at 300 K. Simulated annealing was undertaken upon completion of the dynamics simulations, by repeat minimisation of the dynamics output using the CG algorithm until the structure would minimise no further.

5.4. Minimisation studies of C.I. Reactive Red 2 within a water matrix

A C.I. Reactive Red 2 molecule was constructed within the molecular editor of the Quanta 97® package, this structure was then subjected to gas phase minimisations over 4000 iterations using the SD, then CG algorithms. This structure was then solvated, with a 30 Å box of water, using the solvation option within the calculation menu. The resultant model was then re-minimised as until the structure would minimise no more initially by SD, then by CG methods.

5.5. Molecular dynamics studies of C.I. Reactive Red 2 within a water matrix

Solvated dynamics simulations were studied by performing dynamics simulations on the model generated from procedure 3. The simulations were carried out as in our previous paper using 4 ps time scale for each of the dynamic simulation components.

5.6. Re-minimisation and dynamics simulations of cellulose microfibril [19]

Using a model of a section of a cellulose microfibril which was previously constructed [19] it was possible to re-minimise the structure and perform dynamics simulations as outlined earlier within Quanta 97® to check that similar results were obtained to those of O'Sullivan [19].

5.7. Molecular dynamics simulations of urea in the presence of a cellulose matrix

Using a model of a section of a cellulose microfibril which was previously constructed [19] it was possible to place urea molecules in close proximity to the side edges of the cellulose block. These structures were then solvated with a 10 Å solvation sphere, and the models subjected to repeated minimisations using the CG algorithm until the structure would minimise no further. The structure was then subjected to dynamics simulations lasting 12 ps in total before simulated annealing by re-minimisation as outlined previously.

5.8. Molecular dynamics simulations of two C.I. Reactive Red 2 molecules in the presence of a cellulose matrix

Using a model of a section of a cellulose microfibril which was already constructed [19] it was possible to place two C.I. Reactive Red 2 dye molecules in the vicinity of the edges of this cellulose block. The structure was then solvated with a 10 Å solvation sphere; this was then subjected to repeated minimisations using the CG algorithm until the structure would minimise no further. The structure was then subjected to dynamics simulations lasting 4 ps before re-minimisation.

5.9. Additive construction, minimisation and dynamics

Additive molecules were constructed using the 2D molecular editor interface within Quanta 97®. Each structure was then subjected to gas phase minimisations over 4000 iterations using the steepest descent (SD) algorithm to remove high energy interactions, then the minimisation was repeated using the conjugate gradient (CG) algorithm again until the structure reached its minimum energy according to the CHARMm force field. Using the CG minimisation output from above, molecular dynamics simulations were performed. The dynamics simulations were run over a 4 ps time scale, for each of the stages, heating to 300 K, equilibration and simulation at 300 K. Simulated annealing was undertaken upon completion of the dynamics simulations, by repeat minimisation of the dynamics output using the CG algorithm until the structure would minimise no further.

5.10. Cellulose–additive probe mapping

Probe maps were performed using the interaction mapping menu within Quanta 97®. The two structures *i.e.* the cellulose and the chosen additive that had both previously been minimised and taken part in dynamics simulations and annealing studies were opened and the additive chosen to be the probe whilst the dye was chosen as the structure to be probed within the confines of a 10 Å box and $+100$ kcal mol^{-1} and -200 kcal mol^{-1}. The process was then left to run overnight before the probe maps were displayed as a grid around the cellulose matrix.

References

[1] (a) Flower KR, Hamlin JD, Whiting A. Mol Simul 2002;28:1031–41;
(b) Hamlin JD, Whiting A. Mol Simul 2005;31:605–12.
[2] Marchessault RH, Liang CY. J Polym Sci 1962;59:357–60.
[3] (a) Horii F, Hirai A, Kitamura R. Polymers for fibres and elastomers. ACS Symp Ser 1987;340:119–20;
(b) Dudley RL, Fyfe CA, Stephenson PJ, Deslandes Y, Hamer GK, Marchessault RH. J Am Chem Soc 1983;105:2469–70;
(c) Horii F, Hirai A, Kitamura R. Macromolecules 1986;19:930–3.
[4] Atalla RH, Vanderhart DA. Cellulose and wood: chemistry and technology. In: Proceedings of the 10th cellulose conference. Wiley; 1989. p. 169–75.
[5] Ahmed AU, Ahmed N, Aslam J, Atta MA, Butt NM, Khan QH. J Polym Sci Polym Lett Ed 1976;14:561–4.
[6] Herbert JJ, Muller LLJ. J Appl Polym Sci 1974;18:3373–6.
[7] Fengel D, Stoll M. Wood Sci Technol 1989;23:85–9.
[8] Hanley J, Giasson J, Gray DG, Revol JF. Polymer 1992;33:4639–42.
[9] O'Sullivan AC. Cellulose 1997;4:173–6.
[10] (a) Allinger NL. J Am Chem Soc 1977;99:8127–31;
(b) Powell MJD. Comput J 1964;7:155–8;
(c) Scott RA, Scheraga HA. J Chem Phys 1965;42:2209–12.
[11] (a) Hardy B, Sarko A. Polymer 1966;37:1833–7;
(b) Hardy B, unpublished results.
[12] Chanzy H. Proceedings of the international symposium on wood and pulp chemistry, vol. 1. 1987. p. 235–8.
[13] Zenkov ID, Zalepukhin RV, Slovetskii VI, Papkov SP. Vysokomol Soedin A 1988;30:1718–20.
[14] Baird MS, O'Sullivan AC, Banks WB. Cellulose 1998;5:89–92.
[15] Li TQ, Henrikson U, Ödberg L. Cellulose and wood: chemistry and technology. In: Proceedings of the 10th cellulose conference. Wiley; 1988. p. 403–6.
[16] (a) Yano S, Rigdahl M, Kolseth P, de Ruvo A. Svensk Papperstid 1985;88:10–3;
(b) Kohata K, Moygawa M, Takaoka A, Kawai H. Sen-I Gakkishi 1986;42:136–8.
[17] Pizzi A, Eaton NJ, Bariska M. Wood Sci Technol 1987;21:235–8.
[18] (a) Peemoeller H, Sharp AR. Polymer 1985;26:859;
(b) Khamrakulov G, Myagova NV, Budtov VP. Polym Sci Ser B 1994;36:698–701.
[19] O'Sullivan AC. PhD thesis. Bangor, UK: UCNW; 1995.
[20] Hartley ID, Kamide FA, Peemoeller H. Wood Sci Technol 1992;26:83–6.
[21] Goring DAI. In: Fibre–water interactions in paper making. The British Paper and Board Industry Federation; 1978. p. 2–8.
[22] Schuerch C, Davidson RW. J Polym Sci Part C 1971;231–5.
[23] Stamm AJ. Forest Prod J 1955;413.
[24] Mannan KHM. Polymer 1993;34:2485–8.
[25] (a) Kissa E. Text Res J 1969;39:734–7;
(b) Achwai WB. Colourage 1992;39:33–5.